Reconfigurable Switching Network for Multimode Fiber Arrays

Ray T. Chen, Michael R. Wang and Tomasz Jannson

Physical Optics Corporation
2545 West 237th Street, Suite B
Torrance, California 90505

and

Robert Baumbick

NASA Lewis Research Center
Cleveland, OH 44135

ABSTRACT

We report the first electro-optic switching device compatible with multimode fibers. A 1-to-many cascaded reconfigurable interconnection was built.

A thin glass substrate was used as the guiding medium which provides not only higher coupling efficiency from multi-mode fiber to waveguide but also better tolerance of phase matching conditions. Involvement of a TIR hologram and multi-mode waveguide eliminates interface problems between fibers and waveguides. The DCG holographic material has proven to be reliable from -180°C to +200°C. Survivability of such an electro-optic system in harsh environments is further ensured. $LiNbO_3$ was chosen as the E-O material becuase of its stability at high temperatures (phase transition temperature >1000°C) and maturity of E-O device technology. Further theoretical calculation was conducted to provide the optimal interaction length and device cpacitance.

1. INTRODUCTION

Optical fiber arrays have been proposed for signal paths in various civilian and military controls as a means of offering advanced sensing functions not available in electronic systems, reducing the weight of a control system, and eliminating electromagnetic interference (EMI). Optical fiber data transmission lines and a myriad of sensors have been developed [1-4] for such applications. To implement optic fiber sensors on various control systems, a proper electro-optic architecture (EOA) needs to be studied. Among the many EOAs that have been investigated [5] (such as multiple sources and multiple detector (MSMD) topology, single source and multiple detector (SSMD) topology, multiple sources and single detector (MSSD) topology, and single source and single detector (SSSD) topology), SSSD topology seems to be the most promising. Figure 1 shows a feasible electro-optic architecture for this application. The number of light sources and detectors are minimized in this case; however, to realize such an EOA, proper electro-optic switching elements are needed to multiplex (receiver) and demultiplex (transmitter) optical carriers in the time domain so that the specific direction where proper fiber sensors or receivers are located can be selected. To date, most integrated optic switches are not compatible with multi-mode fibers [6-8] when employing data or for short distance communication, i.e., within a ship or an airplane. Therefore, there exists a need to develop a new electro-optic switch to overcome the above shortages.
Fiber Optic technology offers numerous well known benefits including the capability for high bandwidth operation, low weight and immunity to man made threats such as Electromagnetic Interference (EMI) and

Electromagnetic Pulses (EMP) generated by nuclear blasts. DOD and NASA have recently sponsored several programs to promote research and development in the areas of fiber optic sensor technology.

Optical fiber sensing devices have so many advantages over other types of sensing devices that they have become the focus of a significant amount of research. Physical parameters such as position, velocity, acceleration, temperature, pressure, vibration, voltage, current, etc., can be successfully measured via fiber optic sensor technology. Table 1 lists fiber sensor technologies that are available today. Both U.S. government agencies such as DOD and NASA and private industries such as Boeing, McDonnell Douglas and Hughes Aircraft Company are eagerly pursuing optical sensor devices and systems. The multiple mode switching system we built in this program shall encompass all these different scenarios of fiber sensor technologies. Since the communication distance from the sensors to the processing unit is relatively short (within the plane), multi-mode fiber is selected to route the sensed signals.

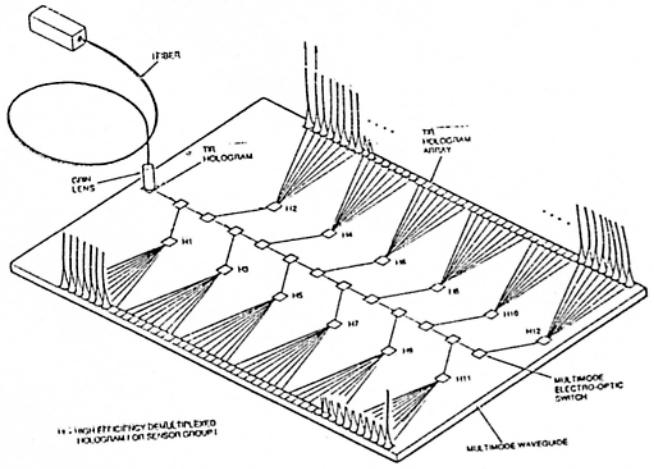

Figure 1 Electro-Optic Architecture for Multi-Mode Fiber Sensor Array.

The major bottleneck for the implementation of multi-mode fiber sensor arrays is the mismatch between existing electro-optic switching devices and multiple mode fiber. This issue becomes more difficult when the power budget is strictly limited. The existing multi-mode optical switches fall into two categories: moving fiber and scanning optical beam. There are three fundamental problems which preclude their use in high speed multiplexer for the reconfigurable massive fan-out sensor systems which are to be implemented. These intrinsic limitations are:

1. Low fan-out/fan-in capability. The moving fiber and scanning technologies basically provide 1-to-1 interconnection. Beam scanning provided by an acoustic Bragg cell can provide hundreds of resolvable spots. However, such a device can only provide reconfigurable 1-to-1 interconnection. The usefulness of the A-O scanner depends on the electro-optic architecture and the number of sensors to be used. In the case of a small interconnection system where the number of sensors involved is relatively small, the A-O scanner may be a proper candidate.

2. High insertion loss. The losses associated with the moving fiber and scanner are high, which makes the system insertion loss unacceptable. This kind of loss is mainly induced by beam divergence, Fresnel reflection, scattering and mode mismatch.

3. Slow switching speed. Moving fibers involve the adjustment of mechanical parts and the speed is intrinsically slow. Scanner devices, except the A-O Bragg cell, have the same problems as moving fibers. Fast switching speed is important for fast access of the sensor signal.

Table 1 Fiber Optic Sensor Technology Availability

	Rotary Position	Linear Position	Angular Velocity	Tachometer/ Shaft Speed	Linear Acceleration	Temperature	Pressure	Flow (Mass)	Voltage	Current	Flow (Volume)	Liquid Level	Pyrometer	Flame Sensor	Clearance	Proximity Switch	Vibration
TDM Digital Optical Code Plate	●	●					●										
WDM Digital Optical Code Plate	●	●															
Analog Gradient Filter Plate	●	●															
Beam Interrupt/Pulse Count	●	●		●													●
Microbend Modulated					●		●										●
Absorption Edge Shift						●											
Reflective Diaphragm						●	●	●			●				●	●	●
Near Total Internal Reflection												●					
Farady Effect						●				●							
Raman/Raleigh Backscatter						●											
Blackbody Radiation						●											
Passive IR Analysis						●							●	●			
Fabry-Perot Interferometer						●	●		●	●							
Phosphorescent						●											
Fluorescent						●											
E-O Diffraction Grating							●		●					●			●
Michelson Interferometer							●		●								
Mach-Zehnder Interferometer					●				●								●
Sagnac Interferometer			●			●											
Photo-Elastic							●										
Power-By-Light (PBL)	●	●				●										●	

In this paper, we report a new type of electro-optic switch which provides massive fan-out/fan-in capability, low insertion loss and high switching speed and compatibility with multi-mode fiber. An electro-optic switching array proposed to meet the requirements of the electro-optic architecture (Figure 1) is shown in Figure 2. The whole system is built on a multiple mode glass waveguide which relays the optical signal from light sources such as laser diodes and LEDs to fiber sensor arrays. The selection of the optical wave from light sources to a specific sensor or sensor array is controlled by the cascaded multiple mode electro-optic switching array shown in Figure 2.

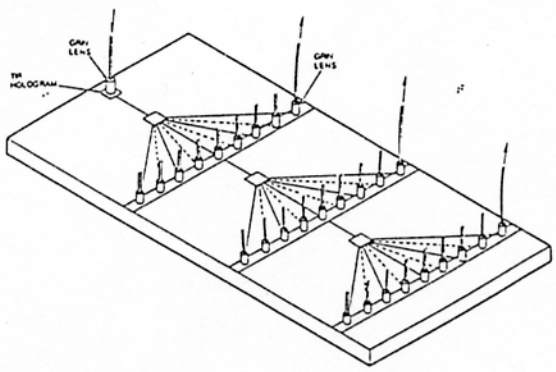

Figure 2 Cascaded Switching Array Using Raman-Nath Electro-Optic Gratings.

2. ELECTRO-OPTIC SWITCHING DEVICE FOR MULTI-MODE FIBER SENSOR ARRAY

2.1 State-of-the-Art Electro-Optic Switching Devices

Integrated electro-optic modulators have been studied for more than two decades. Electro-optic modulation of light can be separated into phase, polarization, and intensity modulation. One of the most popular types is the directional coupler [9,10]. Because of the overlap in the evanescent fields of two waveguides, light couples between them with a coupling coefficient depending on the waveguide parameters, wavelength, and inter-waveguide separation. With the proper conditions, all of the light entering one waveguide can couple to the other. By electro-optically producing an index difference between the two waveguides, light which crosses over at different points along the directional coupler is no longer in phase and the net cross-over efficiency can be made zero. Another modulation scheme is the integrated optic version of the Mach-Zehnder interferometer [11,12] with one input channel and one output channel. It was first reported by W. E. Martin in 1975 [11]. This type of modulator employs the interference of coherent light going through different lengths of optical path which can be controlled by external bias. The throughput intensity will be modulated due to the phase difference. Four other promising waveguide modulators are the cutoff [13,14], phase [15], total internal reflection (TIR) [16], and X switches [17].

Each of the above intensity modulators has been demonstrated on insulating and semiconductor substrates. All of them employ thin film dielectric waveguides as the fundamental building blocks with a combination of properly designed electrode patterns. A high frequency, wide bandwidth electro-optic modulator of up to 20 GHz at 1.3 μm has been achieved [18]. A modulator array with 500 channels/cm packing density on GaAs-GaAlAs heterostructure has also been published. Each channel has more than a 2 GHz modulation bandwidth [19].

The brief description above reflects that the existing switching devices in integrated optics are compatible only with single-mode fiber. Except for the technology developed in this program, integrated optic switching devices are intrinsically not compatible with multi-mode fiber due to the different guiding layer geometries between multi-mode fiber and single-mode waveguides.

2.2 Electro-Optic Switch Compatible with Multi-Mode Fiber

To solve the aforementioned interface problems, we developed a novel electro-optic grating switch architecture which is capable of matching well with multi-mode fiber. Phase gratings can be directly induced in electro-optic materials through the use of interdigitated electrodes on the surface of the electro-optic material. The E-O grating working in the single-mode scenario is well known in integrated optics. It is not compatible with multi-mode fiber. The outstanding concept of the proposed architecture is that it implements a well-known device on a thin low-index plate, typically 10-100 mils. The plate is used as the guiding medium to route optical waves from light sources to the desired locations where fiber sensors are located. A comparison of the integrated-optic grating switch and the newly proposed E-O grating is shown in Figure 3. Figure 3(a) shows the traditional integrated optic electro-optic grating switch. The guiding medium is typically from submicron to a few microns. Typical multi-mode fiber has a core diameter of 100 μm and it is obvious that compatibility between these two devices is not possible. The proposed E-O switch is shown in Figure 3(b). The output beam profiles of the developed device and multi-mode fiber are extremely well matched. The result will be demonstrated in Section 4.0.

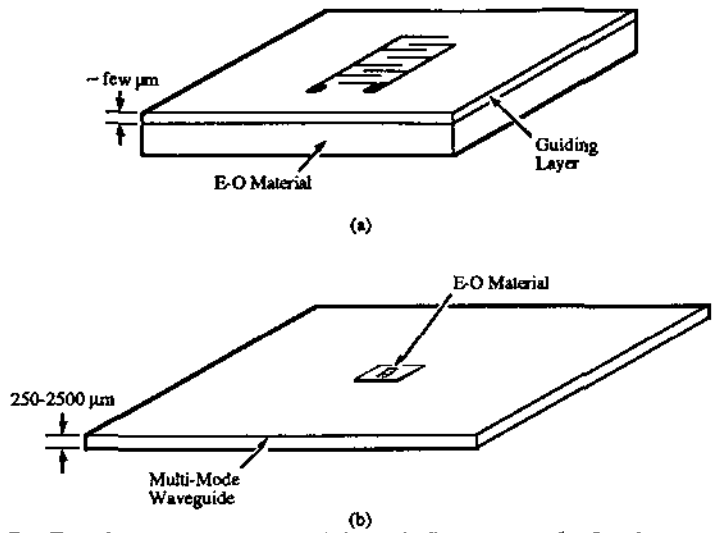

Figure 3 E-O Grating in (a) Traditional Integrated Optics and (b) Newly Proposed Architecture.

2.2.1 Theory of Operation

Beam diffraction, as a mechanism for intensity modulation by electro-optic means in thin films, is achieved by producing an electrically controlled phase grating in the path of the propagating beam. The diffraction process results from a periodic perturbation of the refractive index transverse to the beam propagation direction. A useful method for electro-optically generating the desired phase grating is shown in Figure 4. The mechanism for interaction relies on the fringes of electric fields extending below the surface between interdigital strip electrodes formed on the crystal surface. The local fringing field strength should be reasonably uniform across the guided beam and approximately sinusoidal in the plane of the guiding layer, transverse to the beam.

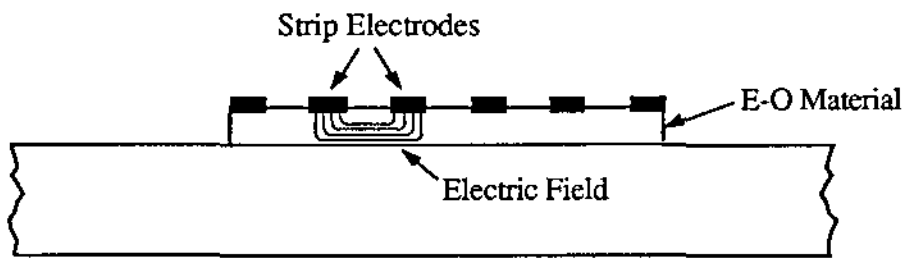

Figure 4 Phase Grating Formation by the Electro-Optic Effect.

This may be most readily achieved by applying an isolating lower-index layer above the guiding layer. This serves the added function of minimizing the interaction of the optical beam evanescent tail with the lossy metallic surfaces. Bragg diffraction involves introducing the input beam at a specific angle θ_B, the Bragg angle, with respect to the electrode array [20,21]. Diffraction occurs reflectively in a single output at twice the input angle when the Bragg condition is satisfied

The phase change ϕ, in radians, induced by the electrical signal field over a pathlength L is

$$\phi = [(2\pi L)/\lambda_o]\,\Delta n \qquad (2\text{-}1)$$

where Δn is the refractive index increment caused by the electro-optic effect and λ_o is the free-space wavelength. The strongest interaction in uniaxial crystals, such as $LiTaO_3$ and $LiNbO_3$, occurs when the applied electric field and optical electric polarization are both parallel, or nearly parallel [20], to the crystalline *c* axis (optic axis). For this condition, the refractive-index increment is

$$\Delta n_3 = \frac{1}{2} n_e^3 r_{33} E_3 \tag{2-2}$$

where n_e is the extraordinary refractive index, r_{33} is the appropriate electro-optic coefficient, and E_3 is the applied electric field [22]. Thus, the crystal must be cut with its *c* axis in the plane of the waveguide essentially transverse to the beam propagation direction, and the propagating optical mode must have TE polarization. This polarization has the least loss characteristics in proximity to the metal electrode surfaces. Thus, this minimizes the insertion loss of the modulator which was caused by absorption. Combining Eqs. (2-1) and (2-2) yields

$$\phi = \frac{\pi L n_3^3 r_{33} E_3}{\lambda_o} \tag{2-3}$$

Assume that the *c* -axis-oriented electric field in the region of the guided layer is approximately sinusoidal in the transverse direction (a reasonable assumption for a region about a distance *s* below the surface). For Bragg diffraction, the zero- and first-order powers are proportional, respectively, to $\cos^2(\phi/2)$ and $\sin^2(\phi/2)$. For modulation, corresponding to 100% depletion of the zero-order beam in the idealized case, the maximum required value of ϕ is π.

2.2.2 Interaction Length

In our device, the optical wave bounces up and down as shown in Figure 5. The interaction length I_L, i.e., the length over which index modulation exists, is

$$I_L \lesssim \frac{d}{\cos\theta} \tag{2-4}$$

where d is the thickness of the electro-optic material and θ is the bouncing angle. To evaluate the interaction length we need to first compute the electric field distribution which is related to index modulation by Eq. (2-2).

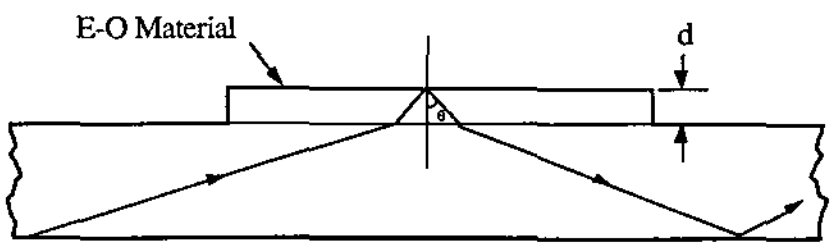

Figure 5 *Side View of Beam Propagation.*

The electrode configuration for which the change in refractive index will be computed is shown in Figure 6. Two semi-infinite electrodes are deposited on a $LiNbO_3$ surface. The electrodes are assumed to be

infinitely thin compared to the distance a. One electrode is at zero potential while the other electrode is at potential U. The orientation of the crystal is such that the a, b and c axes are parallel to the y, z and x axes, respectively. For this crystal orientation the permitivity tensor is diagonal so that the electrostatic potential V is the solution of the following differential equations:

$$\frac{\partial^2 V}{\partial x^2} + \frac{\partial^2 V}{\partial y^2} = 0 \qquad \text{for} \quad y > 0 \tag{2-5}$$

$$\varepsilon_x \frac{\partial^2 V}{\partial x^2} + \varepsilon_y \frac{\partial^2 V}{\partial y^2} = 0 \qquad \text{for} \quad y < 0 \tag{2-6}$$

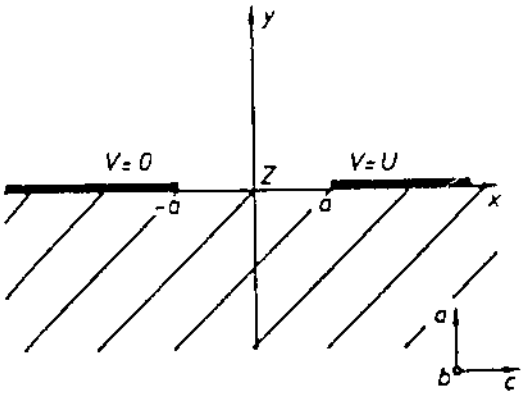

Figure 6 Electro-Optic Light Modulator Configuration with Two Semi-Infinite Electrodes.

The change in dielectric constant introduced by the optical guiding layer is so small that it can be neglected for the computation of the electrostatic fields. Using the coordinate transformation

$$y' = \sqrt{\frac{\varepsilon_x}{\varepsilon_y}}\, y \tag{2-7}$$

Eq. (2-6) can be written as

$$\frac{\partial^2 V}{\partial x^2} + \frac{\partial^2 V}{\partial y'^2} = 0 \qquad \text{for} \quad y < 0 \tag{2-8}$$

The boundary conditions are V = 0 and V = U on the electrodes, together with the required continuity across the dielectric-air interface of the normal component of the dielectric displacement and the tangential component of the electric field.

Assume that the Laplace equation has been solved for the same electrode configuration as shown in Figure 6, but without the dielectric. One can easily see that the solutions for $V_a(x,y)$ and $V_a(x,y')$ are ensured by the fact that $y = y' = 0$ at the interface. The potential V is therefore related to the potential V_a by

$$V(x,y) = V_a(x,y) \qquad \text{for } y > 0 \tag{2-9}$$

$$V(x,y) = V_a(x, y') \qquad \text{for } y < 0 \tag{2-10}$$

The potential V_a for the homogeneous case can easily be found using conformal mapping techniques [23, 24]. The conformal transformation:

$$z = a \cosh w \tag{2-11}$$

where:

$$z = x + jy$$
$$w = u + jv$$

or

$$x = a \cosh u \cos v$$
$$y = a \sinh u \sin v$$

maps the configuration of Figure 6 into a parallel plate structure. The upper electrode has a potential π, while the lower electrode is at zero potential.

The potential V in the crystal is therefore given by

$$V(x,y) = \frac{U}{\pi}\left[\pi - v(x,y')\right] \tag{2-12}$$

The components of the electric field in the crystal can now be written as

$$E_x = -\frac{1}{a}\,\frac{\cosh u \sin v}{\cosh^2 u - \cos^2 v}\,\frac{U}{\pi}$$

$$E_y = \frac{1}{a}\,\frac{\sinh u \cos v}{\cosh^2 u - \cos^2 v}\,\frac{U}{\pi}\sqrt{\frac{Ex}{Ey}} \tag{2-13}$$

The change in refractive index Δn_x is proportional to the x component of the electric field

$$\Delta n_x = -\frac{1}{2}\, n_x^3\, r_{33}\, E_x \tag{2-14}$$

One can now compute Δn_x at any point in the crystal by means of Eqs. (2-11) to (2-14). Contour lines for $(a/U)\Delta n_x$ are plotted in Figure 7 for the case of a $LiNbO_3$ crystal ($r_{33} = 31 \times 10^{-12}$ m/V). Taking, for example, the potential U = 30 V and a = 50 μm, one finds that the contour line indicated by 0.5 corresponds to a change in refractive index of 3×10^{-5}.

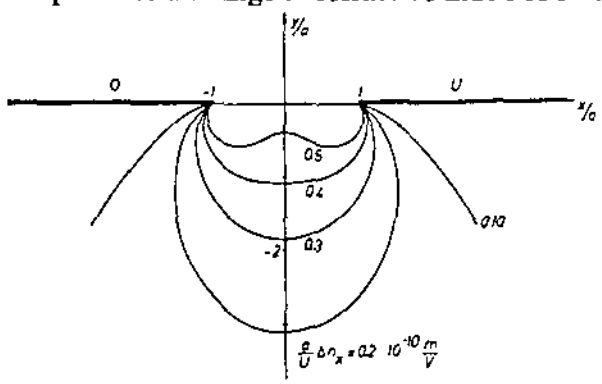

Figure 7 *Contour Lines for $(a/U)\Delta n_x$, for the Electrode Configuration Shown in Figure 6.*

The penetration depth of Δn_x is an important factor in assessing the interaction length and therefore modulation efficiency for a guided mode. From Eq. (2-13) one can obtain a very simple expression for the variation of E_x along the negative y axis. This is

$$E_x = \frac{-U}{\pi\sqrt{y'^2 + a^2}} \tag{2-15}$$

In practice, semi-infinite electrodes are not used, but the solution presented above is a very good approximation for the case where the gap between the electrodes is much smaller than the electrode width. Detailed theoretical results based on interdigital electrode array can be found in Reference 25.

3. EXPERIMENTAL RESULTS

We constructed for the first time a $LiNbO_3$ electro-optic switch built on a glass substrate which serves as a multi-mode waveguide. The switch was designed to fit into the EOA shown in Figure 1-1. The schematic of this switching device is shown in Figure 2. The device was designed with a short interaction length and a small electro-optic grating vector **K**. Accordingly, the Raman-Nath type [28] diffraction scheme was expected.

3.1 Compatibility with Multi-Mode Fiber

In Figure 2, the cascaded fiber arrays are situated so that various diffraction orders can be successfully coupled into preselected fibers. The electro-optic grating was designed so that

$$\mathbf{K}_{out} = \mathbf{K}_{in} + n\,\mathbf{K}$$
$$n = 0, \pm 1, \pm 2, \cdots \tag{3-1}$$

where K_{out} and K_{in} are defined as:

$$K_{out} = K_{in} = \frac{2\pi}{\lambda} \tag{3-2}$$

and **K** is the electro-optic grating vector. The electro-optic grating we employed for this application has a grating spacing of $\Lambda = 40\ \mu m$. Many diffraction orders have been observed. It will be noted that the waveguide structure we used in the application is not the conventional type with waveguide dimension close to diffraction limitation (submicron to a few microns). The waveguide mode we defined is sometimes called a substrate mode in integrated optics. We define this type of device as a multi-mode waveguide for two reasons: 1) the optical wave is guided and propagated in a well defined direction and 2) all optical waves that satisfy total internal reflection conditions can be guided modes defined herein. One of the most important results in employing this type of waveguide is that the insertion loss for coupling between waveguide and multi-mode fiber is extremely low (< -0.5 dB/joint). The mode profile of this multi-mode waveguide, which used thin glass substrate as the guiding medium, is well matched with the near field pattern of guided modes of multi-mode fiber. The near field pattern of the guided mode of these two guided wave devices are shown in Figure 8. The waveguide mode was coupled out through a total internal reflection (TIR) hologram. The interface problem we described in the beginning of this paper is therefore solved due to the continuity of the guided mode profiles of these two different devices.

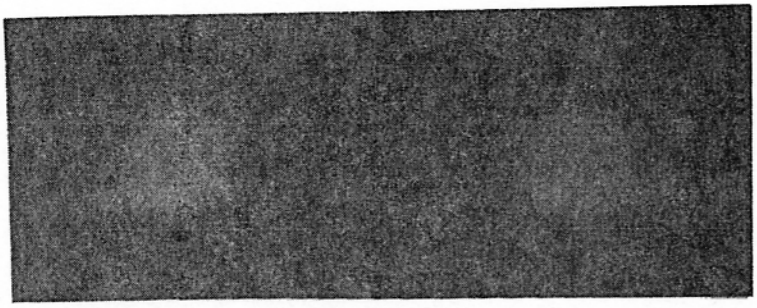

Figure 8 Near Field Patterns of the Guided Wave of Multi-Mode Fiber (Left) and Multi-Mode Glass Waveguide (Right) (100 μm in Diameter).

3.2 Integration of Electro-Optic Switching Elements

Demonstration of the whole package including input multi-mode fiber, GRIN lens, TIR input hologram, glass waveguide, $LiNbO_3$ electro-optic grating and TIR output coupler is shown in Figure 9. The index of refraction of lithium niobate is higher than glass and, therefore, the guided mode in the glass substrate penetrated through the $LiNbO_3$ and interacted with the active region of the E-O grating located on the top surface of $LiNbO_3$. The electrode was made of Cr/Al. Accordingly, a diffraction grating existed when there was no external E field added (static grating effect). Use of such a grating can provide a 1-to-many fiber sensor interconnection. If this type of interconnection is not desired, the electrode should be made of transparent materials such as ITO (Indium Tin Oxide). There is no static grating effect in this case. 1-to-many fan-out is provided only by external voltage. Application of an external voltage generated a refraction index modulation due to the Pockel effect. The external field was added along the C-axis (z) of the crystal and the generated index modulation Δn is

$$\Delta n = \frac{1}{2} r_{33} n^3 E \qquad (3\text{-}3)$$

where r_{33} is the associated electro-optic coefficient. The grating space used is quite large (40 μm) and it is expected that a few hundred volts were required to switch off the 0th order light. The far field image of many diffraction orders at $V = 0$ and $V = 350$ volts is shown in Figure 14. The existence of diffraction at $V = 0$ volts is due to the static grating slits generated by the Ar/Al electrode. Figure 14 was taken at an image plane perpendicular to the output TIR grating coupler. An array of bright spots is clearly observed. Each individual spot corresponds to one output fiber which routes the optical wave to the site where the sensing device is located.

3.3 Switching Speed and Power Budget

The switching speed of the electro-optic grating switch was limited by the capacitance of the device. In the case of a lumped electrode structure with $R = 50$ ohms impedance termination, the modulation bandwidth is given by $T = 2\pi/\Delta f$.

The capacitance of the planar electrodes was calculated using the conformal mapping method. With $R = 50$ ohms, there is 130 MHz modulation bandwidth which corresponds to ~50 nsec switching time ($T = 2\pi/\Delta f$). The speed is much faster than that of moving fibers and scanning devices. The electro-optic grating used has 80 fingers. Further increase of switching speed can be successfully achieved by reducing the number of fingers. A switching network compatible with FDDI standards is achievable.

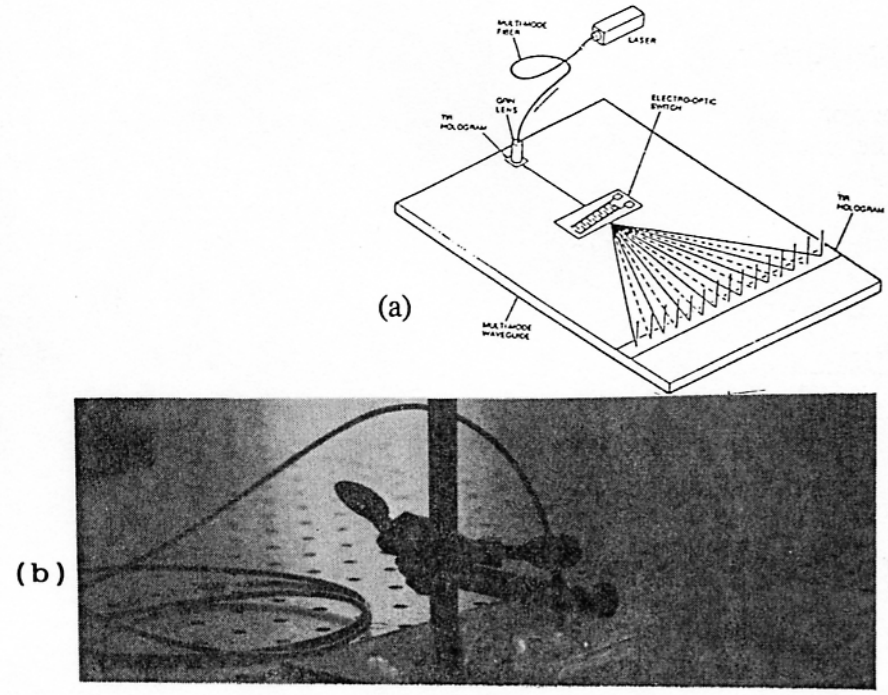

Figure 9 (a) Demonstration of the Multi-Mode Switch; (b) Schematic of (a). photo

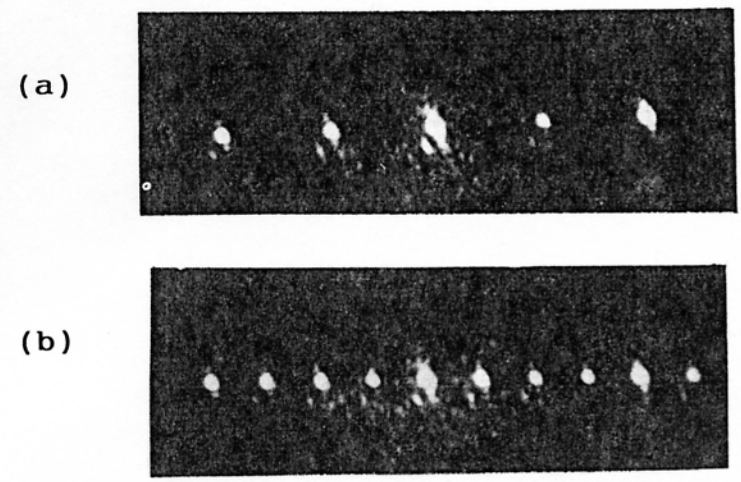

Figure 10 Far Field Image of Diffracted Light at (a) V = 0 and (b) V = 350 Volts. The existence of diffraction at V = 0 volt is due to the Cr/Al electrode.

The usefulness of each individual spot depends upon the power budget of each sensor system. The elements of the optical power budget are the source power intensity, the insertion losses of the interconnection network, and the signal to noise ratio required to obtain the desired level of sensor performance/sensitivity. For fiber-optic sensors, a wide dynamic range receiver is usually required, so a PIN photodiode with a transimpedance type preamplifier is the receiver design of choice. For digital sensors, the signal to noise ratio must be at least 12 to achieve a bit error rate better than 10^{-9}.

This data actually determines the minimum power level needed at the receiver end. The combination of these data with other loss factors such as coupling and propagation loss determines the minimum input power required for each spot.

3.4 Massive Fanout Hologram

The total number of interconnection points, i.e., the number of fiber sensors involved will determine the final size of the package. Massive fan-out interconnection is provided by a highly multiplexed transmission hologram (HMTH). Each HMTH routes optical signals to a specific group of fiber sensors. A 1-to-20 massive fan-out optical interconnect working in a multiple mode glass waveguide is shown in Figure 11. Each individual streak corresponds to one fan-out signal to be relayed to the site where a specific fiber sensor is located.

Figure 15 1-to-20 Massive Fan-Out Using a Multiplexed Planar Hologram.

4. CONCLUSION

In summary, we achieved the first electro-optic grating switch for a multi-mode optical fiber sensor array. A 1-to-many cascaded reconfigurable interconnection was built based on this technology. A thin glass substrate was used as the guiding medium which provides not only higher coupling efficiency from multi-mode fiber to waveguide but also better tolerance of phase matching conditions. Involvement of a TIR hologram and multi-mode waveguide eliminates interface problems between fibers and waveguides. The DCG holographic material has proven to be reliable from -180°C to +200°C. Survivability of such an electro-optic system in harsh environments is further ensured. $LiNbO_3$ was chosen as the E-O material because of its stability at high temperatures (phase transition temperature >1000°C) and maturity of E-O device technology. Further theoretical calculation was conducted to provide the optimal interaction length and device capacitance.

The electro-optic grating was designed in the Raman-Nath regime to provide a 1-to-many interconnection. Reconfigurability was provided by independently switching on and off each switching device shown in Figure 1. Application of an ITO transparent electrode can eliminate the diffraction at V = 0 volts.

The aforementioned technologies such as high efficiency TIR holograms, electro-optic gratings, and multi-mode glass waveguides, are well established. The electro-optic architecture (EOA) reported herein is new and compatible with multi-mode fiber sensor array systems. A low cost and highly reliable multi-mode switching network for fiber sensor arrays can be constructed based on the technologies described herein.

5. REFERENCES

1. Stanton, R. O. April 1983. "Digital Optical Transducers for Helicopter Flight Control Systems," SPIE Proc., 412, 122.

2. Farina, J., R. Hubbard, and P. Lefkowitz. 1983. Development and Test of a Digital/Optical Rotary Position Transducer. USSAAVRADCOM TR 83-D-15, U.S. Army Research and Technology Laboratories, Ft. Eustis, VA.
3. Poumakis, D. J., and W. J. Davies. December 1986. Fiber Optic Control System Integration Final Report. Report No. CR 179569.
4. Russell, J. C., et al. 1986. "Protocol Branch Optimization Method used in FOCSI Program Fiber Optic Control System," IECE Japan OFS'86 Technical Digest, 3.
5. Glomb, W. L. Electro-Optic Architecture (EOA) for Sensors and Actuators in Aircraft Propulsion Systems, Final Report, NASA Contract Number NAS3-25343.
6. Ishida, K., H. Nakamura, R. Matsumura, T. Kadoi, and H. Inoue. 1987. "InGaAsP/InP Optical Switches Using Carrier Induced Refractive Index Change," Appl. Phys. Lett., 50, 141.
7. Tonchev, S., and I. Savatinova. 1985. "Optical Multimode X-Switch in Ti-Diffused $LiNbO_3$," J. of Optical Communications, 6, 3.
8. Lorenzo, J. P., and R. A. Soref. 1987. "1.3 mm Electro-Optic Silicon Switch," Appl. Phys. Lett., 51, 6.
9. Papuchon, M., et al. 1975. "Electrically Switched Optical Directional Coupler: Cobra," Appl. Phys. Lett., 27, 289.
10. Alferness, R. C., R. V. Schmidt, and E. H. Tuner. 1979. "Characterization of Ti-diffused $LiNbO_3$ Optical Directional Couplers," Appl. Opt., 18, 4012.
11. Martin, W. E. 1975. "A New Waveguide Switch/Modulator for Integrated Optics," Appl. Phys. Lett., 32, 562
12. Ramaswamy, V., M. D. Divino, and R. D. Standley. 1978. "Balanced Bridge Modulator Switch Using Ti-Diffused $LiNbO_3$ Strip Waveguides," Appl. Phys. Lett., 32, 644-646.
13. Chen, R., and C. S. Tsai. 1986. "Thermally Annealed Single-Mode Proton-Exchanged Channel Waveguide Cut Off Modulator," Opt. Lett., 11, 546.
14. Chen, R. 1989. "Thermally Annealed Mode Annihilation Switching Array on Proton Exchanged $LiNbO_3$ Channel Waveguides," SPIE, San Diego, CA.
15. Chang, C. L., and C. S. Tsai. 1983. "Electro-Optic Analog-to-Digital Convertor Using Channel Waveguide Fabry-Perot Modulator Array," Appl. Phys. Lett., 43, 22.
16. Tsai, C. S., B. Kim, and F. R. El-Akkari. 1978. "Optical Channel Waveguide Switch and Coupler Using Total Internal Reflection," IEEE J. Quantum Electron., QE-14, 539
17. Neyer, A. 1983. "Electro-Optic X-Switching Using Single-Mode Ti:$LiNbO_3$ Channel Waveguides," Electron. Lett., 19, 533.
18. Wang, S. Y., S. H. Lin, and M. Huong. 1987. "GaAs Traveling-Wave Polarization Electro-Optic Waveguide Modulator with Bandwidth in Excess of 20 GHz at 1.3um," Appl. Phys. Lett., 51, 83.
19. Chen, Ray T., et al. 1987. "GaAs-GaAlAs Heterostructure Single-Mode Channel Waveguide Cutoff Modulator and Modulator Array," IEEE J. of Quantum Electron., QE-23, 2205.
20. Hammer, J. M., and W. Phillips. 1974. Appl. Phys. Lett., 24, 545.
21. Noda, J., N. Uchida, and T. Saku. 1974. Appl. Phys. Lett., 25, 13.
22. Chen, F. S. 1970. IEEE Proc., 1440.
23. Moon, P., and D. E. Spencer. 1961. Field Theory Handbook. Springer Verlag, Berlin.
24. Durand, E. 1966. Electorstatique. Masson, Paris.
25. Ray T. Chen, "Multiple Mode Electo-optic Networks," Final Report to joint program office of National Aerospace plane, Contract No. F33657-89-C-2208.